Available online at www.CivileJournal.org

Civil Engineering Journal

(E-ISSN: 2476-3055; ISSN: 2676-6957)

Vol. 11, No. 05, May, 2025

Fire Behavior of Concrete Beams Reinforced with Various Combinations of GFRP and Steel

Det Van Doan [1, 2], Vui Van Cao [1, 2*]

[1] *Faculty of Civil Engineering, Ho Chi Minh City University of Technology (HCMUT), District 10, Ho Chi Minh City, Vietnam.*

[2] *Vietnam National University Ho Chi Minh City, Linh Trung Ward, Thu Duc City, Ho Chi Minh City, Vietnam.*

Received 21 November 2024; Revised 11 April 2025; Accepted 16 April 2025; Published 01 May 2025

Abstract

This paper investigates the effects of key parameters on the fire resistance of concrete beams reinforced with various combinations of glass fiber-reinforced polymer (GFRP) and steel. The ratio of GFRP area (A_f) to the total area (A) of GFRP and steel varied from 0 to 1, making steel, hybrid GFRP-steel, and GFRP-reinforced concrete (RC) beams. Finite element models of these beams were developed in SAFIR software and verified. The models were then used to analyze the effects of different key parameters on the fire behavior and fire resistance of these beams. The results demonstrated that the fire behavior of these beams was significantly affected by the A_f/A ratio, load ratio, total reinforcement ratio, and concrete cover thickness, while it was marginally affected by steel and concrete strengths. The fire resistance decreased with the increases in load ratio and A_f/A ratio, whereas it increased with the increases in concrete cover thickness or reinforcement ratio. Fire resistance slightly increased with the increase in the tensile strength of steel and slightly decreased with the increase in the compressive strength of concrete. The location arrangement of GFRP and steel bars in cross sections significantly affected the fire behavior and fire resistance of hybrid beams. The deflection rate limit, rather than the deflection limit, decisively governed the fire resistance of concrete beams reinforced with different A_f/A ratios. Regression analyses yielded models for estimating the fire resistance.

Keywords: GFRP; GFRP-Steel Reinforcement; Reinforced Concrete Beam; Fire; Fire Resistance; SAFIR.

1. Introduction

Steel-reinforced concrete (RC) structures are widely used in construction; however, steel reinforcement is susceptible to corrosion [1, 2] in aggressive environments. To overcome this drawback, fiber-reinforced polymer (FRP) was used to replace steel reinforcement because of its outstanding characteristics, such as high tensile strength, light weight, and high corrosion resistance. However, FRP presents elastic behavior until rupture without exhibiting the yielding stage, resulting in brittle failure. In addition, FRP commonly has a lower elastic modulus than steel; therefore, FRP RC members or structures can have more cracks and larger deflections than steel RC ones. A solution to avoid both possible brittle failure and corrosion is to combine both FRP and steel for reinforcement. This solution also improves both the strength and ductility of hybrid FRP-steel RC beams.

Narrowing the topic to concrete beams reinforced with combinations of steel and FRP, the behavior and mechanical properties of these beams at ambient temperature have been widely investigated by the research community. Ge et al. [3] investigated the flexural behavior of BFRP-steel RC beams. Experiments were conducted on five BFRP-steel RC beams. The results indicated that the decrease in the BFRP-to-steel area ratio decreased the deflection of hybrid BFRP-

* Corresponding author: cvvui@hcmut.edu.vn

http://dx.doi.org/10.28991/CEJ-2025-011-05-018

steel RC beams. The ductility of BFRP-steel RC beams can satisfy the requirement when the BFRP-to-steel ratio is appropriate. El Refai et al. [4] investigated the performance of hybrid GFRP-steel RC beams. Experiments were conducted on six hybrid GFRP-steel RC beams and three GFRP RC beams. The results indicated that concrete beams over-reinforced by combinations of GFRP and steel had higher strength and ductility than those reinforced with only GFRP. Pang et al. [5] analyzed the mechanical properties of hybrid FRP-steel RC beams. They concluded that the increase in the equivalent reinforcement ratio detrimentally affected the ductility of these hybrid beams. Additionally, GFRP bars provided higher ductility for hybrid RC beams than other FRP types. Qin et al. [6] investigated the flexural performance of hybrid FRP-steel RC beams, considering the effect of reinforcement ratio. The results confirmed the significant influence of FRP-to-steel area ratios on the ductility and strength. An FRP-to-steel area ratio of 1.0–2.5 was recommended for design to ensure the stiffness and ductility. Barris et al. [7] tested twelve GFRP RC beams and found that these beams failed at relatively large deflections. The ultimate loads obtained from the experiments were 51% and 17% higher than those obtained based on ACI 440.1R-06 [8] and Eurocode 2 [9], respectively. This can be due to the ultimate compressive strain adopted in these codes being lower than the real ultimate strain. The results also indicated that GFRP RC beams had high deformation capacity in spite of the brittle failure of concrete crushing in the compression zone. Qu et al. [10] investigated the behavior of eight hybrid GFRP-steel RC beams. The test results indicated that these hybrid beams had good ductility and strength.

Lau & Pam [11] tested twelve concrete beams, including concrete beams, steel RC beams, FRP-RC beams, and FRP-steel RC beams. The results indicated that hybrid FRP-steel RC beams had higher ductility than FRP RC ones. Stirrups with 135° increased the ductility but did not affect the strength. Kara et al. [12] presented a method to predict the flexural behavior of FRP-steel RC beams. Sectional analysis was performed to obtain moment–curvature curves, which were used to compute the deflection and the moment capacity. The result also indicated that the increase in steel ratio increases the ductility and stiffness of hybrid FRP-steel RC beams. Araba and Ashour [13] experimentally investigated the flexural behavior of continuous GFRP-steel beams. The results indicated that the increase in GFRP ratios at regions of negative and positive moments increased the load-carrying capacity but reduced the ductility. The increase in steel ratios at critical sections increased the ductility but lessened the increase in load-carrying capacity after steel yielded. The plastic hinge mechanism at mid-span and the middle support can be used to estimate the load-carrying capacity of hybrid GFRP-steel RC beams. Duic et al. [14] studied the behavior of BFRP RC beams and compared it with that of steel RC beams. The results indicated that BFRP RC beams with a low BFRP ratio exhibited more flexural and shear cracks than steel RC beams. BFRP RC beams had acceptable deformations. The crack moment of BFRP RC beams was 30–50% lower than that of steel RC beams. Abbas et al. [15] studied the influence of the ratio and configuration of GFRP and steel on the flexural behavior of GFRP-steel RC beams. The results indicated that the increase in steel ratio improved the ductility and serviceability. The performance of hybrid GFRP-steel RC beams using ultra-high-performance concrete [16], concrete beams reinforced with various FRP types [17, 18], cracked hybrid GFRP-steel RC beams retrofitted with CFRP [19], or GFRP-steel RC beams under impact loading [20] was also investigated. Therefore, combinations of these two materials for reinforcement of concrete structures are a good engineering solution because they improve both strength and ductility at ambient temperature.

However, fire causes different negative effects on the behavior and mechanical properties of structures [21, 22] in general. Masood & Nadjai [23] investigated the behavior of CFRP and hybrid CFRP-steel RC beams in fire. Six beams with dimensions of 120 × 200 × 2000 mm were tested under four-point loading with a load ratio of 0.4. The research results showed that the tested beams failed in flexure, while the hybrid steel-CFRP RC beams exhibited better ductile behavior and stiffness than conventional steel or FRP RC beams. Two layers of CFRP reinforcement provided the highest load-carrying capacity but lowest ductility for the beams. Rafi & Nadjai [24] used DIANA software to model the behavior of CFRP and hybrid CFRP-steel RC beams in fire. They proposed constitutive laws to adequately capture the behavior of these beams exposed to fire. They found that the arrangement of CFRP and steel bars affected the fire resistance of hybrid beams. The thickness of concrete cover significantly affected the fire resistance of beams. Tian et al. [25] studied the fire resistance of hybrid FRP-steel RC beams. They proposed a method to calculate the strength reduction coefficient of reinforcement of concrete beams. Based on the allowable reduction coefficient and properties of sections and materials, a method to determine the fire resistance of hybrid RC beams was proposed. Tests of fire resistance were carried out for six hybrid GFRP-steel beams, and the obtained fire resistances were close to those calculated using the proposed method.

Albu-Hassan & Al-Thairy [26] investigated the behavior of hybrid GFRP-steel RC beams after exposure to elevated temperatures. Experiments were conducted on seven hybrid GFRP-steel RC beams and one control beam with dimensions of 250 × 160 × 1125 mm. Two concrete types were used: lightweight concrete in the tension zone and normal concrete in the compression zone. The beams were heated to 300°C, 350°C, 500°C, and 700°C. Experimental results indicated that the failure mode of these heated beams was caused by shear failure. Exposure to 700°C reduced the strength by 53% and the ductility by 12% compared with that of the control beam. Al-Thairy [27] developed a simplified method to predict the failure modes and behavior of hybrid GFRP-steel RC beams in fire. The method was based on the strain compatibility and the force equilibrium on sections of beams subjected to bending moments, considering the reductions in material properties at high temperatures. The method was verified and used for parametric studies. When GFRP bars and steel bars were arranged in the two layers in the tension zone, respectively, the ultimate load-carrying capacity increased by 35% compared with the case of one-layer arrangement. Hassan et al. [28] experimentally studied the behavior of eight hybrid basalt FRP (BFRP)-steel RC beams after exposure to 500°C for 2 hours. The studied main parameter was the ratio of BFRP area to steel area. The results indicated that BFRP-steel RC beams had higher shear strength and crack stiffness, while it mitigated the brittle failure. Due to the higher ductility and absorbed energy of BFRP RC beams after exposure to fire, BFRP reinforcement was more effective than steel reinforcement. The authors also encouraged further studies to justify their observations.

Saafi [29] analyzed the effect of fire on concrete members reinforced by FRP and developed models to compute the flexural strength and shear strength of FRP RC beams. These models employed the reductions in strengths of concrete and FRP due to fire. The studied parameters included the concrete cover and fire duration. The results revealed that the temperature of FRP reduced when the concrete cover thickness increased. The flexural strength and shear strength declined significantly. Said et al. [30] used hybrid bars (steel bars covered with GFRP) and GFRP-steel combinations as reinforcement for concrete beams. They found that the stiffness of GFRP-steel RC beams exposed to constant 300°C and 600°C for one hour was reduced by 17% and 31% compared with that of beams reinforced with hybrid bars. Mamdouh et al. [31] examined the shear performance of GFRP-reinforced beams exposed to fire and found that the shear resistance decreased with the increase in the flexural reinforcement and fire duration. Fire performance of only-steel RC members [32] or only-GFRP RC structural members [33] has also been conducted. Recently, Rosa et al. [34] extensively reviewed different aspects of only-GFRP RC structural members exposed to fire.

The above review indicates that studies on the behavior of hybrid FRP-steel RC beams at ambient temperature overwhelmed those at high temperature, e.g., exposure to fire. Hybrid FRP-steel RC beams may suffer from several issues when these structures are exposed to fire. These issues have not been fully understood due to a limited number of studies published in the literature. The effects of key parameters on the fire resistance of concrete beams reinforced with various combinations of GFRP and steel still need to be clarified. To this end, this paper aimed at the fire behavior and the fire resistance of concrete beams reinforced with various combinations of GFRP bars and steel bars. To achieve this aim, finite element models were developed in SAFIR software. The results obtained from these models were verified by comparing them with the available experimental results, with good approximations. These models were then used for parametric studies. The parameters included: 1) the ratio (A_f/A) of GFRP area (A_f) to the total area of steel and GFRP (A), 2) the total reinforcement ratio (ρ), 3) the load ratio, 4) the thickness of concrete cover, 5) the yield strength of steel (f_y), 6) the compressive strength of concrete (f'_c), and 7) the locations of GFRP bars and steel bars. The results were analyzed and compared to come to conclusions.

2. SAFIR Modeling

SAFIR is specialized software for simulating structures exposed to fire. This software incorporates the nonlinear finite element method in 2 stages. Stage 1 is the thermal analysis, in which the temperature distributions in sections are established. Stage 2 is the mechanical analysis, taking into account the simultaneous effects of load and temperature.

2.1. Thermal Modeling

A 2D thermal model was used for thermal analysis. Beam dimensions, thermal parameters of concrete, steel, and GFRP materials, and fire conditions were taken into account in the model. The STEELEC2EN model was used for steel and GFRP. Other parameters, such as convection coefficient in hot surfaces (convection coeff hot), convection coefficient in cold surfaces (convection coeff cold), relative emission, elastic modulus, and Poisson ratio, were the default values incorporated in the software. CONCEC 2020 model, which is based on Eurocode 2 [9], was used for concrete. Parameters of the concrete model include specific mass, water content, coefficient of convection on heated surfaces, coefficient of convection on cold surfaces, emissivity, elastic modulus, Poisson ratio, and thermal conductivity. Thermal characteristics are taken according to the default model in SAFIR software.

2.2. Structural Modeling

A structural 2D model was used to analyze the mechanical and thermal behavior of RC beams exposed to fire. The distribution of temperature on the cross section of beams in a 2D thermal model was used to analyze stress and deformation based on changes in mechanical properties of materials during the fire exposure. Normal concrete (NS CONCRETE) was used for modeling. The concrete was made from the siliceous-based rock, which was modeled as SILCON_ETC material in SAFIR. Its parameters include Poisson ratio, compressive strength, and tensile strength.

Exposed to fire, the strength of concrete is reduced with the increase in temperature. The reduction coefficient of compressive strength of concrete (k_c) recommended by Eurocode 2 [9], as shown in Equation 1, was used, in which T is the temperature.

$$\begin{aligned} &k_c = 1 \quad if \quad T \le 100°C \\ &k_c = 1.067 - 0.00067T \quad if \quad 100°C \le T \le 400°C \\ &k_c = 1.44 - 0.16T \quad if \quad 400°C \le T \le 900°C \\ &k_c = 0 \quad if \quad 900°C \le T \end{aligned} \tag{1}$$

The reduction in elastic modulus of concrete exposed to fire recommended by Gernay & Franssen [35], as expressed by Equation 2, was used for the modelling.

$$\begin{aligned} &k_{Ec} = 1.0233 - 0.0018 \quad if \quad T \le 300°C \\ &k_{Ec} = 0.8038 - 0.001T \quad if \quad 300°C \le T \le 600°C \\ &k_{Ec} = 0.2517 - 9 \times 10^{-5}T \quad if \quad 800°C \le T \end{aligned} \tag{2}$$

Carbon steel, in accordance with Eurocode 2 [9], was used for modeling. Its properties include elastic modulus, Poisson coefficient, and ultimate strength. At high temperatures, the yield strength and elastic modulus decrease with respect to the temperature, as expressed by Equations 3 and 4, respectively [9].

$$\begin{aligned} &k_s = 1 \quad if \quad T \le 350°C \\ &k_s = 1.889 - 0.00257T \quad if \quad 350°C \le T \le 700°C \\ &k_s = 0.24 - 0.002T \quad if \quad 700°C \le T \le 1200°C \\ &k_s = 0 \quad if \quad 1200°C \le T \end{aligned} \tag{3}$$

$$\begin{aligned} &k_{Es} = 1 \quad if \quad 0 \le T \le 100°C \\ &k_{Es} = 1.1 - 0.001T \quad if \quad 100°C \le T \le 500°C \\ &k_{Es} = 2.05 - 0.0029T \quad if \quad 500°C \le T \le 600°C \\ &k_{Es} = 1.39 - 0.0018T \quad if \quad 600°C \le T \le 700°C \\ &k_{Es} = 0.41 - 0.0004T \quad if \quad 700°C \le T \le 800°C \\ &k_{Es} = 0.27 - 0.000225T \quad if \quad 800°C \le T \le 1200°C \\ &k_{Es} = 0 \quad if \quad 1200°C \le T \end{aligned} \tag{4}$$

GFRP material was modeled using USER_STEEL model, which is a type of reinforcement with a linear stress-strain relationship up to ultimate, while the reduction coefficients were assigned by users. As suggested by Saafi [29], the reduction coefficient of tensile strength (k_f) and elastic modulus (k_{Ef}) of GFRP are expressed by Equations 5 and 6, respectively. To avoid computational problems with zero strength and modulus after 400°C, small values (close to zero) were assigned for these two parameters.

$$\begin{aligned} &k_f = 1 - 0.0025T \quad if \quad 0 \le T \le 400°C \\ &k_f = 0 \quad if \quad 400°C \le T \end{aligned} \tag{5}$$

$$\begin{aligned} &k_{Ef} = 1 \quad if \quad 0 \le T \le 100°C \\ &k_{Ef} = 1.25 - 0.0025T \quad if \quad 100°C \le T \le 300°C \\ &k_{Ef} = 2 - 0.005T \quad if \quad 300°C \le T \le 400°C \\ &k_{Ef} = 0 \quad if \quad 400°C \le T \end{aligned} \tag{6}$$

3. Verifications

The SAFIR model was verified by comparing with the experimental results available in the literature.

3.1. RC beams Exposed to Fire

Deflection–time behavior of an RC beam exposed to fire experimentally obtained by Song et al. [36, 37] was used for verification. The RC beam had a cross section of 250 × 400 mm, an overall length of 4 m, and a span length of 3.6 m. The equivalent compressive strength of concrete at 28 days was 25.8 MPa. The tensile reinforcement was 4 ϕ25, while the compressive reinforcement was 2 ϕ16. The yield strengths of steel ϕ16 and ϕ25 were 445 MPa and 451 MPa, respectively. The stirrup was steel ϕ8 with spacings of 150 mm and 200 mm. The thickness of the concrete cover was 25 mm. The beam was simply supported and tested under four-point loading. The distance from the two concentrated loads to the nearest supports was 745 mm. The dimensions of the tested beam are presented in Figure 1.

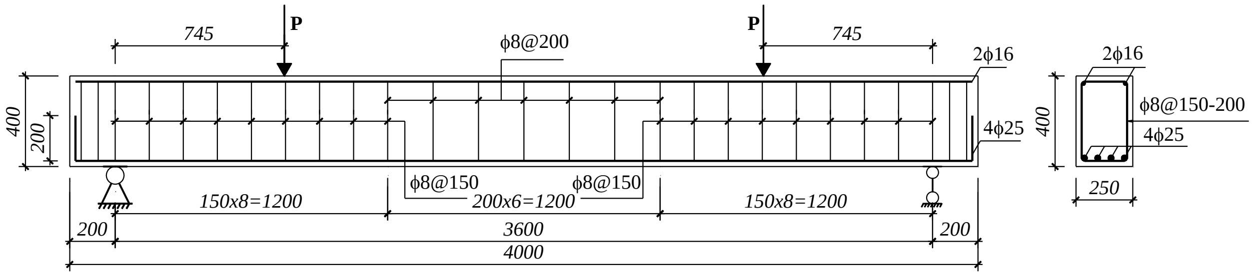

Figure 1. Tested beam B2 [36, 37] (unit: mm)

Table 1 shows the parameters and thermal characteristics of concrete and reinforcement used for 2D thermal modeling in SAFIR software. Table 2 shows the parameters and thermal characteristics for the thermomechanical analysis stage.

Table 1. Parameters for steel and concrete for 2D thermal modeling

Parameters	Steel rebar	Concrete
Convection coeff hot	25	25
Convection coeff cold	4	4
Relative emission	0.7	0.7
Young's modulus (N/m^2)	2×10^{11}	2.4×10^{10}
Poisson coefficient	0.3	0.2
Specific mass (kg/m^3)		2300
Moisture content (%)		3.45
Thermal conductivity		0.5

Table 2. Parameters of steel and concrete for 2D structural modeling

Parameters	Steel	Concrete
Young' modulus (N/m^2)	2×10^{11}	2.4×10^{10}
Poisson coefficient	0.3	0.2
Yield strength (N/m^2)	4.51×10^{8}	
Compression strength (N/m^2)		2.58×10^{7}
Tensile strength (N/m^2)		3.04×10^{6}
Maximum temperature (°C)	1200	

The beam was exposed to ISO 834 fire. The experimental temperature–time curve in the furnace is shown in Figure 2, in comparison with the ISO 834 fire curve. The bottom and two side surfaces of the beam were exposed to the experimental fire curve obtained by Song et al. [36, 37]. The top surface was not exposed to fire and was assigned by F20. These boundary conditions are shown in Figure 3-a. Figure 3-b shows the meshing of cross sections. Thermal analyses were performed, and the distributions of temperature at 45, 90, 135, and 180 min are shown in Figures 4-a to 4-d, respectively. The temperature in the cross section increased significantly with the increase in the fire duration. These figures also show that, with a similar distance to the beam surfaces, the temperature at corners is higher than at other locations. This distribution of temperature may affect the behavior of the hybrid RC beams because the temperature of reinforcement (GFRP and steel) bars can be different. This observation is considered in Section 4.7.

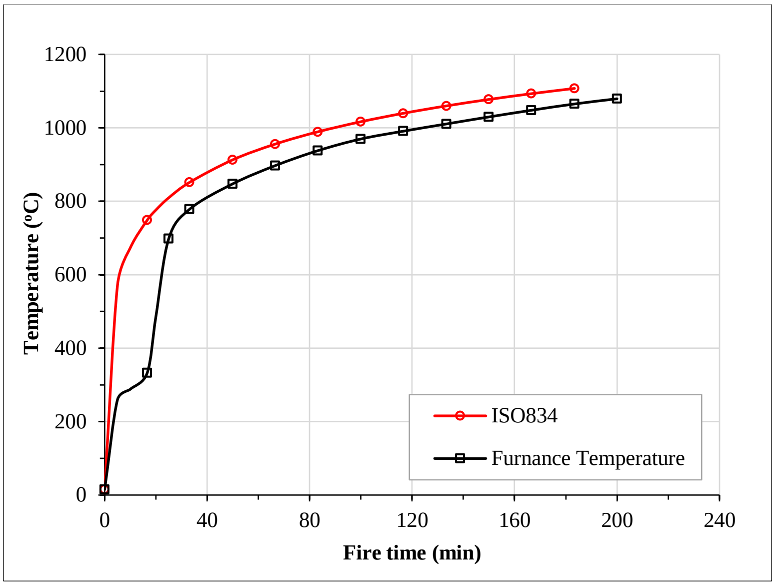

Figure 2. The experimental temperature–time curve obtained by Song et al. [36, 37] versus ISO 834 fire curve

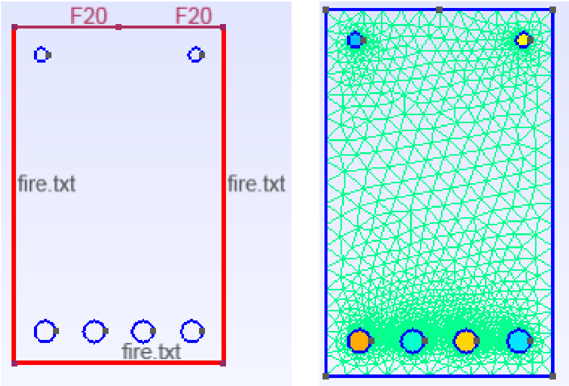

a) Boundary conditions b) Meshing

Figure 3. 2D model for thermal modelling

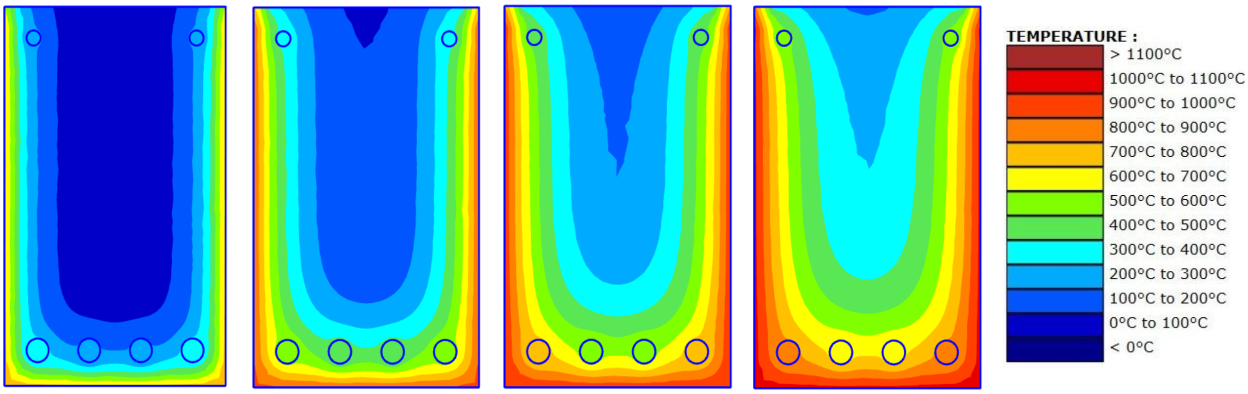

a) 45 min b) 90 min c) 135 min d) 180 min

Figure 4. Distributions of temperature on a cross section at different fire time

The results of thermal analyses were then used for structural analyses. A four-point loading scheme was applied to the beam, as shown in Figure 5. Each of the point loads was 65 kN, applying at 745 mm from the nearest support. Structural analysis was conducted, and the deflections with respect to the fire duration were obtained. Figure 6 compares the results of deflection–time curves obtained from SAFIR and Song et al.'s [36, 37] experiment. This comparison shows a good agreement between the modeling and experimental results. The fire resistance of the beam based on the experiment was 192 min, at which the mid-span deflection was 100.9 mm. Based on the modeling result, the fire resistance was 185 min, at which the mid-span deflection was 103 mm, as shown in Figure 6. The difference in fire resistance of the two results is 3.65%, showing a good accuracy of the SAFIR model.

Figure 5. SAFIR structural model of the simply supported beam under four-point loading

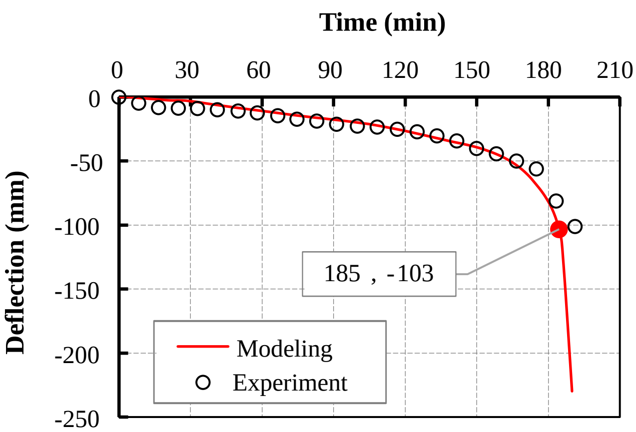

Figure 6. Comparison of deflection–time curves obtained from SAFIR and Song et al. [36, 37]'s experiment

3.2. GFRP RC Beams Exposed to Fire

A GFRP RC beam shown in Figure 7 [38] exposed to fire was modeled by Yu & Kodur [39], and their modeling results were revisited. The beam had a rectangular cross section of 305-mm width and 533-mm height. The beam was simply supported with a span length of 6.01 m. The tensile reinforcement consisted of 8 GFRP bars with a diameter of 19 mm. These eight bars were arranged in two layers. The tensile strength and elastic modulus of GFRP bars were 620 MPa and 44.8 GPa, respectively. The compressive reinforcement was 2 steel bars with a diameter of 12.7 mm. The tensile strength and elastic modulus of steel in the compression zone were 413 MPa and 200 GPa, respectively. The thickness of the concrete cover was 38 mm. The compressive strength of concrete was 34.5 MPa. The beam was subjected to a uniformly distributed load of 27 kN/m, which was 50% of the ultimate load of the beam at ambient temperature. Figure 7 shows the cross-sectional and longitudinal dimensions of the tested beam. Tables 3 and 4 show properties of materials for 2D thermal and 2D structural modeling in SAFIR, respectively.

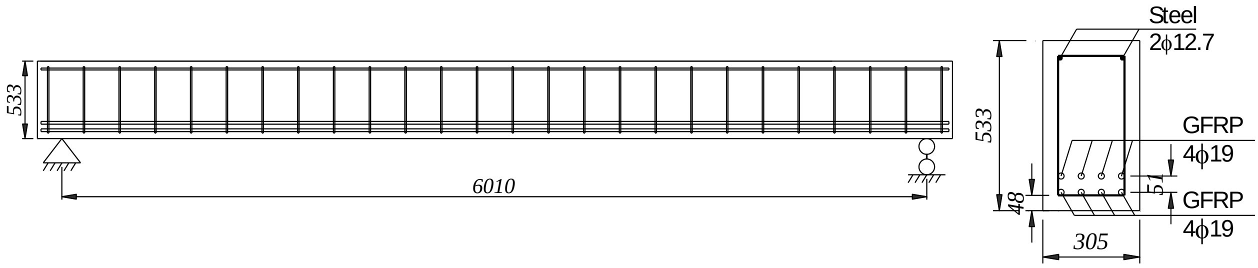

a) Arrangement of reinforcement b) Cross section

Figure 7. Dimensions, reinforcement, and cross section of the modeled beam [38] (unit: mm)

Table 3. Properties of materials for 2D thermal modeling

Parameters	Steel	GFRP	Concrete
Convection coeff hot	25	25	25
Convection coeff cold	4	4	4
Relative emission	0.7	0.7	0.7
Young's modulus (N/m^2)	2×10^{11}	4.48×10^{10}	2.8×10^{10}
Poisson coefficient	0.3	0.28	0.2
Specific mass (kg/m^3)			2300
Moisture content (%)			3.45
Thermal conductivity			0.5

Table 4. Properties of materials for 2D structural modeling

Parameters	Steel	GFRP	Concrete
Young' modulus (N/m^2)	2×10^{11}	4.48×10^{10}	2.8×10^{10}
Poisson coefficient	0.3	0.28	0.2
Yield strength (N/m^2)	3.5×10^{8}		
Ultimate strength (N/m^2)		6.2×10^{8}	
Compression strength (N/m^2)			3.45×10^{7}
Tensile strength (N/m^2)			3.47×10^{6}
Maximum temperature (°C)	1200		

The bottom and two side surfaces of the beam were exposed to ASTM E119 fire, which is similar to ISO 834 fire, while the top surface was not exposed to fire and was assigned the room temperature of 20°C (F20). The boundary conditions are shown in Figure 8-a. Meshing of cross sections is shown in Figure 8-b. Thermal analyses were performed to obtain the distribution of temperature in the cross sections. Figures 9-a to 9-c show examples of temperature distributions at 30, 45, and 60 min, respectively. The phenomenon of temperature concentration at corners is also observed. The effect of this phenomenon on the behavior of beams reinforced with various combinations of GFRP and steel is considered in Section 4.7.

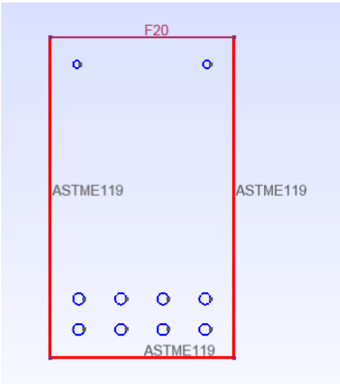

a) Boundary conditions

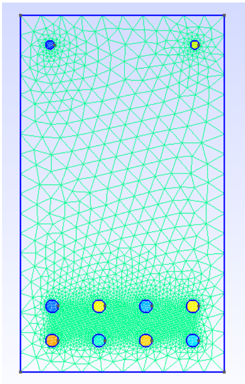

b) Meshing

Figure 8. 2D model for thermal modeling

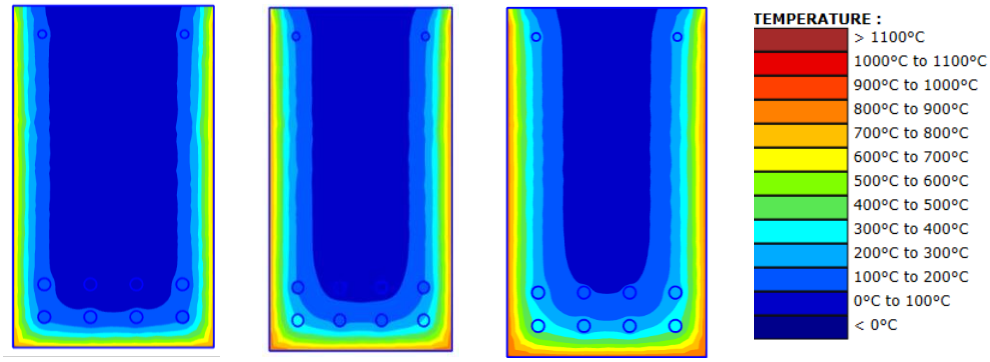

a) 30 min b) 45 min c) 60 min

Figure 9. Distribution of temperature on a cross section at different fire time

The results of thermal analyses were employed for structural analyses. Figure 10 shows the SAFIR model of the simply supported beam under a distributed load of 27 kN/m. Figure 11 shows the deflection–time relationship of the beam obtained from SAFIR modeling in comparison with that modeled by Yu & Kodur [39]. The results indicated that the SAFIR modeling curve is lower than that modeled by Yu & Kodur [39]. A slightly large difference was observed in the duration from 15 min to 50 min, while the remaining portion of the two curves exhibited good agreement. Based on the SAFIR modeling result, the fire resistance was 67 min and the deflection was 78 mm. Based on the modeling result obtained by Yu & Kodur [39], the fire resistance was 64 min and the deflection was 70 mm. Therefore, the differences between the modeling result obtained by Yu & Kodur [39] and SAFIR modeling results are 4.7% for the fire resistance and 11.4% for the deflection. These differences indicated that the model can be used for the fire resistance and the corresponding deflection, although there is a discrepancy at the middle portion of the curves.

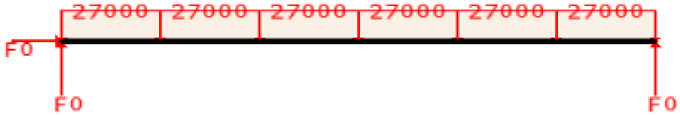

Figure 10. Diagram of the simply supported beam under distributed load

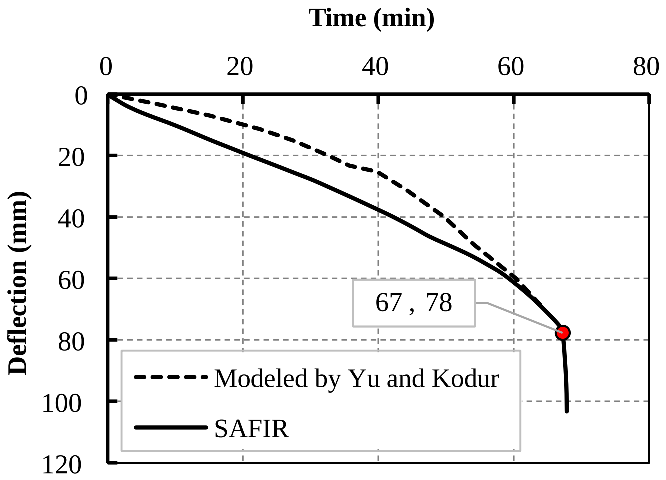

Figure 11. Deflection–time curves: SAFIR modeling vs Yu & Kodur's [39] modeling results

4. Result and Discussion of Parametric Study

After verification, SAFIR models were developed and used for modeling the effects of parameters on the fire resistance of concrete beams reinforced with various combinations of GFRP and steel. Six parameters were considered, including the A_f/A ratio, total GFRP and steel reinforcement ratio (ρ), load ratio (P_a/P_u) of applied load (P_a) to the ultimate load (P_u), concrete cover thickness (a_0), tensile strength of steel (f_y), and compressive strength of concrete (f'_c). Additionally, different locations of GFRP bars on the cross section were also considered. When the effect of one parameter was determined, the other five parameters were kept constant. Two criteria based on the deflection limit and deflection rate were employed. These two criteria were used to determine the fire resistance of beams, whichever occurred first. Based on BS EN1363-1:2020 [40], the deflection limit and deflection rate limit are expressed by Equations 7 and 8, respectively, in which L (mm) is the span length and d (mm) is the effective height of the cross section.

$$\text{Deflection limit: } D = \frac{L^2}{400d} \text{ (mm)} \tag{7}$$

$$\text{Deflection rate limit: } \frac{dD}{dt} = \frac{L^2}{9000d} \text{ (mm/min)} \tag{8}$$

Concrete beams with a cross section of 250 × 350 mm and a span length of 3.5 m were used for the modeling. Various combinations of GFRP and steel were used for the reinforcement of the beams. The beams were subjected to a concentrated load at the mid-span. The steel in the compression zone was 2ϕ14 with a yield strength of 342 MPa. The tensile strength and elastic modulus of GFRP bars were 800 MPa and 45 GPa, respectively. The beam was simultaneously subjected to load and fire.

4.1. Effect of A_f/A Ratio

To consider the influence of the A_f/A ratio on the fire resistance, different A_f/A ratios of 0.0, 0.2, 0.4, 0.6, 0.8, and 1.0 were selected. Concrete had a compressive strength of 30 MPa, and the thickness of concrete cover was 20 mm, measured to the edge of the tensile bars. The yield strength of the longitudinal reinforcement was 350 MPa. The beam was subjected to a concentrated load in the mid-span during the fire exposure. This concentrated load was 40% of the ultimate load at ambient temperature conditions. The total longitudinal reinforcement ratio was ρ = 1.58%. Table 5 shows the configurations of the longitudinal steel/GFRP reinforcement and the corresponding A_f/A ratio. Figures12-a to 12-f show the beam sections with various combinations of steel and GFRP for the reinforcement.

Table 5. Combinations of GFRP and steel reinforcement with different A_f/A ratio

Combination	Reinforcement	GFRP area A_f (mm^2)	Steel area A_s (mm^2)	Total reinforcement area $A = A_f + A_s$ (mm^2)	Ratio A_f/A
1	5S18	0.0	1271.7	1271.7	0.0
2	4S18+1G18	254.3	1017.4	1271.7	0.2
3	3S18+2G18	508.7	763.0	1271.7	0.4
4	2S18+3G18	763.0	508.7	1271.7	0.6
5	1S18+4G18	1017.4	254.3	1271.7	0.8
6	5G18	1271.7	0.0	1271.7	1.0

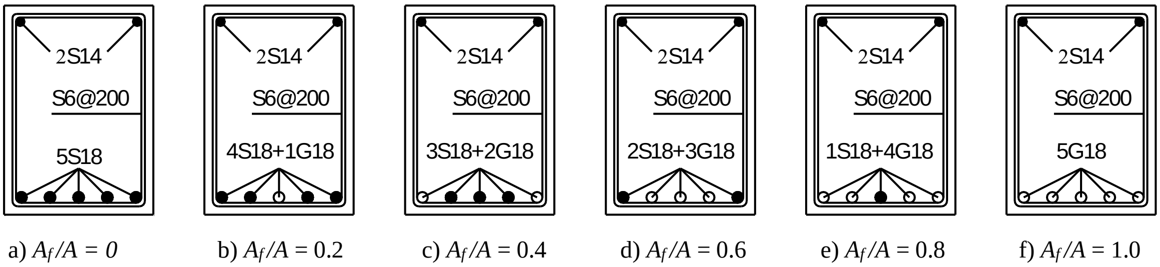

Figure 12. Beams with various combinations of steel and GFRP

Figure 13 shows the deflection–time curves of beams with different A_f/A ratios. In this figure, the round points represent the state that deflection reached the limit deflection of $L^2/400d$, while the square dots present points that the deflection rate reached the value of $L^2/9000d$. This figure indicates that the increase in the GFRP ratio shifted the deflection–time curves leftward, showing a decrease in the fire resistance. For those beams, the limit deflection rate was reached before the limit deflection. The limit deflection can be determined on the curve for the steel RC beam (A_f/A = 0), while other beams did not have this point. The time corresponding to the deflection rate was the fire resistance for these beams.

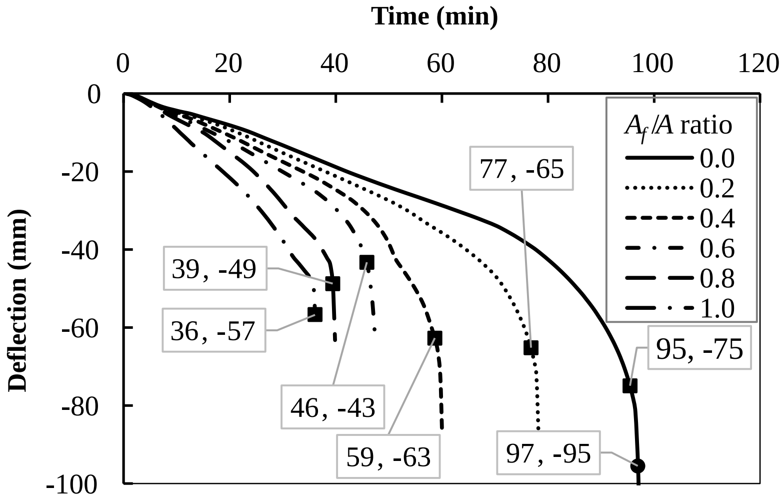

Figure 13. Deflection–time with different A_f/A ratios

Figure 14 shows the fire resistance of RC beams with different A_f/A ratios. This figure indicates that the increase in the A_f/A ratio reduced the fire resistance. This reduction in the fire resistance is attributed to a faster decrease in the tensile strength and elastic modulus of GFRP bars than those of steel bars when the temperature increases. When the ratio A_f/A = 0 (only-steel RC beam), the fire resistance of this beam was 95 min. When this ratio increased to 0.2, the fire resistance decreased to 77 min, reducing 18.9% compared with the fire resistance of only-steel RC beams. When this ratio increased to 0.4, 0.6, and 0.8, the fire resistance significantly decreased to 59, 46, and 39 min, corresponding to a decrease of 37.9%, 51.6%, and 58.9% compared with the fire resistance of only-steel RC beams, respectively. When the ratio is 1.0, the fire resistance of the beam decreases to 36 min, decreasing 62.1% compared with the fire resistance of only-steel RC beams. Figure 14 indicates that when the A_f/A ratio is less than 0.5, the fire resistance decreases linearly with respect to the increase in the A_f/A ratio, and the decreasing rate in fire resistance is about 9 min per A_f/A ratio of 0.1 (on average). When this ratio is greater than 0.5, the decreasing rate in fire resistance decreases significantly up to 2.5 min per A_f/A ratio of 0.1.

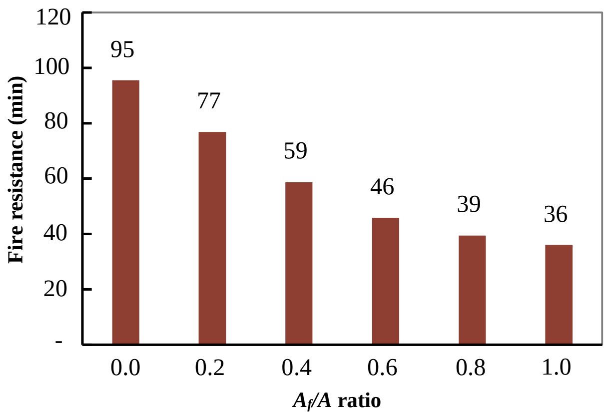

Figure 14. Fire resistance of beams reinforced with different A_f/A ratios

4.2. Effect of Longitudinal Reinforcement Ratio

The reinforcement ratio is an important parameter, directly affecting the failure mechanisms of FRP-steel RC beams. In this subsection, the ratio A_f/A of 0.5 was selected and kept constant, while the total longitudinal reinforcement ratio was changed by increasing the diameter of the steel and GFRP bars. Table 6 shows six configurations of GFRP-steel reinforcement on cross sections and the reinforcement ratio. For example, the configuration of 2S14+2G14 means 2 ϕ14 steel bars and 2 ϕ14 GFRP bars. The third and fourth columns present the ratios ρ_f and ρ_s of GFRP and steel, respectively, while column 5 presents the total reinforcement (both GFRP and steel) ratios. To consider the influence of reinforcement ratio on the fire resistance of beams, other parameters, such as compressive strength of concrete, tensile strengths of steel and GFRP, and thickness of concrete cover, were kept constant. The concentrated load applied during the fire exposure was 40% of the ultimate load at the ambient temperature.

Table 6. Reinforcement ratios

No.	Configuration	ρ_f (%)	ρ_s (%)	$\rho = \rho_f + \rho_s$ (%)
(1)	(2)	(3)	(4)	(5)
1	2S14+2G14	0.380	0.380	0.76
2	2S16+2G16	0.500	0.500	1.00
3	2S18+2G18	0.635	0.635	1.27
4	2S20+2G20	0.785	0.785	1.57
5	2S22+2G22	0.955	0.955	1.91
6	2S25+2G25	1.235	1.235	2.47

Figure 15 shows the deflection–time curves of beams with different longitudinal reinforcement ratios. The increase in the longitudinal reinforcement ratio shifts the curves rightward and upward, showing a significant increase in the fire resistance. Similar to the results in Section 4.1, the fire resistance is governed by the limit deflection rate. The deflections corresponding to the limit deflection rate of these beams are almost similar. Figure 16 shows the relationship between longitudinal reinforcement ratio and fire resistance of the beams. In this figure, the fire resistance increases linearly with the increase in longitudinal reinforcement ratio. However, the increase in the fire resistance with respect to the increase in the longitudinal reinforcement ratio is not significant.

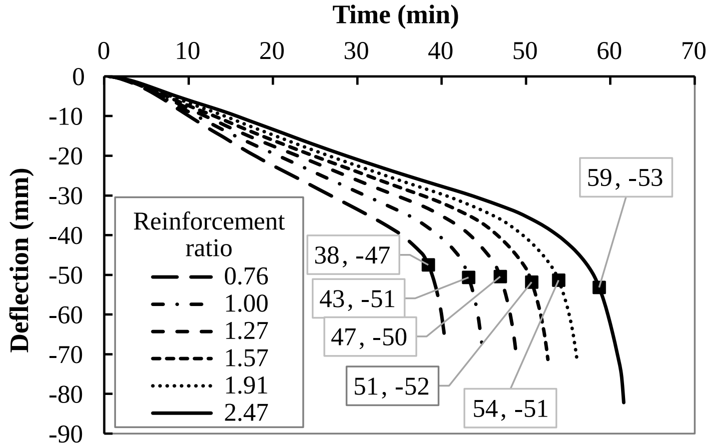

Figure 15. Deflection–time behavior of concrete beams reinforced with different reinforcement ratios

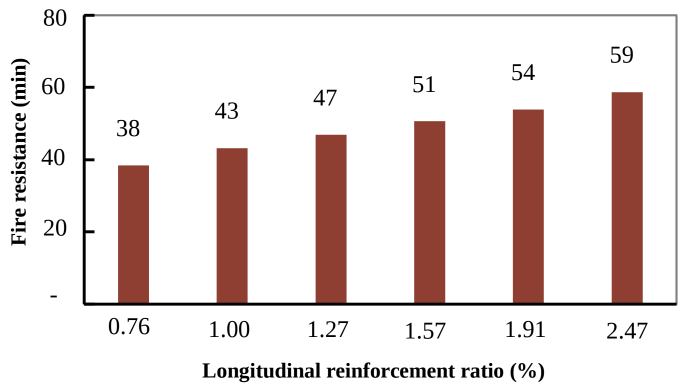

Figure 16. Effect of reinforcement ratio on the fire resistance

Figure 16 shows the variations of fire resistance with respect to the reinforcement ratio. The fire resistance of the RC beam with the reinforcement ratio of 0.76% is 38 min. When the reinforcement ratio is 1%, the fire resistance increases to 43 min, or 13.2%. Further increasing the reinforcement ratio to 1.27, 1.57, 1.91, and 2.47%, the fire resistance increases to 47, 51, 54, and 59 min, which are 23.7, 34.2, 42.1, and 55.3% higher than the fire resistance of the beam with the reinforcement ratio of 0.76%. On average, the fire resistance increases by 1.3 min per reinforcement ratio of 0.1%.

4.3. Effect of Load Ratio

In this subsection, the concrete beam reinforced with 2ϕ18 steel bars and 2ϕ18 GFRP bars was used for modeling. The equivalent reinforcement ratio ρ was 1.27%, and the ratio A_f/A was 0.5. Other parameters, such as the thickness of concrete cover, yield strength of steel, and compressive strength of concrete, were kept constant. The beams were subjected to a constant concentrated load at the mid-span during the fire exposure. The concentrated loads were 10, 20, 30, 40, 50, and 60% of the ultimate load of the beams at ambient temperature, which correspond to the load ratios of 0.1, 0.2, 0.3, 0.4, 0.5, and 0.6, respectively.

Figure 17 shows the deflection–time curves of the beams under different loads. When the load increases, the deflection–time curve shifts leftward, representing a decrease in fire resistance. In addition, similar to the results presented in the above two sections, the fire resistance of the beams is governed by the deflection rate limit. Figure 18 shows the fire resistance of the beams with different load ratios. When the applied load ratio increases, the fire resistance decreases substantially. When the load ratio is 0.1, the fire resistance is 74 min. When this ratio is 0.6, the fire resistance reduces to 41 min, corresponding to a reduction of about 45%. Especially, the reduction rate of fire resistance is the greatest when increasing the load ratio from 0.1 to 0.2: the fire resistance decreases by ~24%. Then, the reduction rate of fire resistance gradually decreases when increasing the load ratio.

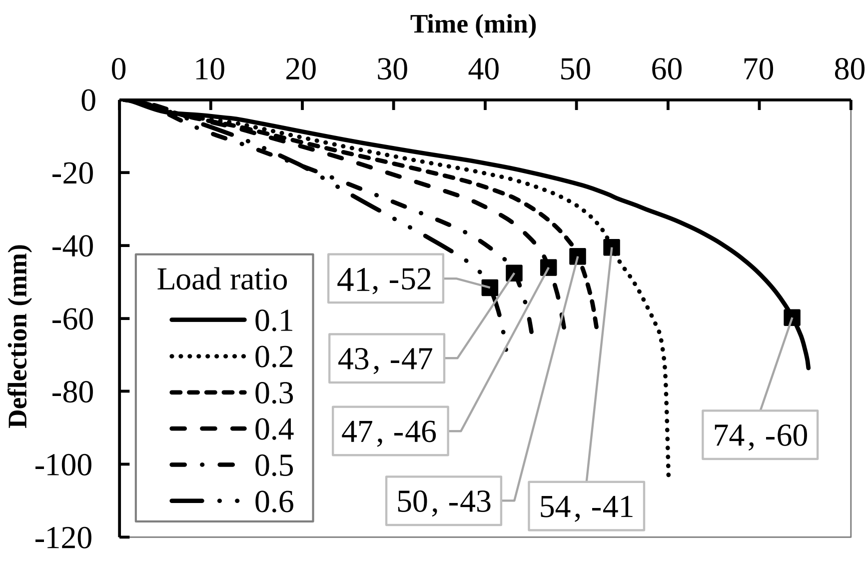

Figure 17. Deflection-time curves of beams with different load ratios

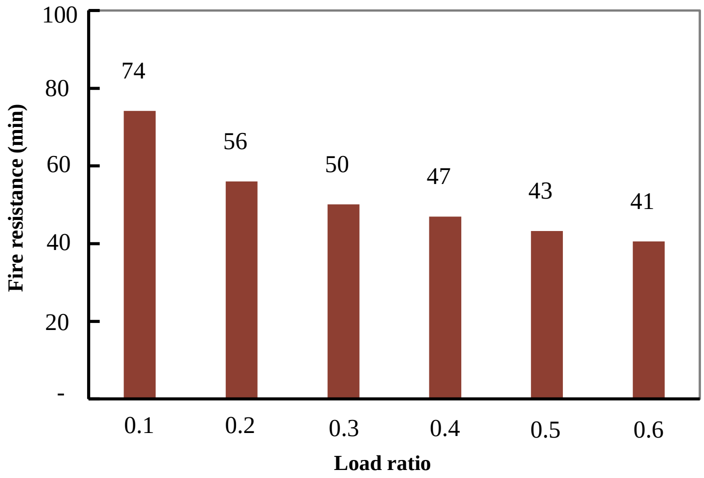

Figure 18. Variation in fire resistance with respect to the load ratio

The higher load caused a higher reduction in the fire resistance. This can be explained by the fact that when the applied load is large, cracks in the concrete develop prior to fire exposure, and more cracks form when the load increases. These cracks provide conditions for the temperature in GFRP/steel reinforcement to increase faster compared with beams under a small load, causing a faster decrease in the strength of GFRP and steel. These more cracks also provide a good condition for the decrease in bond between concrete and GFRP/steel reinforcement at high temperatures, degrading the stiffness and increasing the deflection.

4.4. Effect of Concrete Cover Thickness

In this subsection, the effect of concrete cover thickness on the behavior of the hybrid beams reinforced with 2ϕ18 steel bars and 2ϕ18 GFRP bars was analyzed. The reinforcement and the ratio A_f/A of 0.5 were kept constant. The concrete cover thicknesses were 20, 25, 30, 35, 40, 45, and 50 mm. The load of 40% of the ultimate load was applied to beams during the fire exposure. Figure 19 shows the deflection–time of these beams.

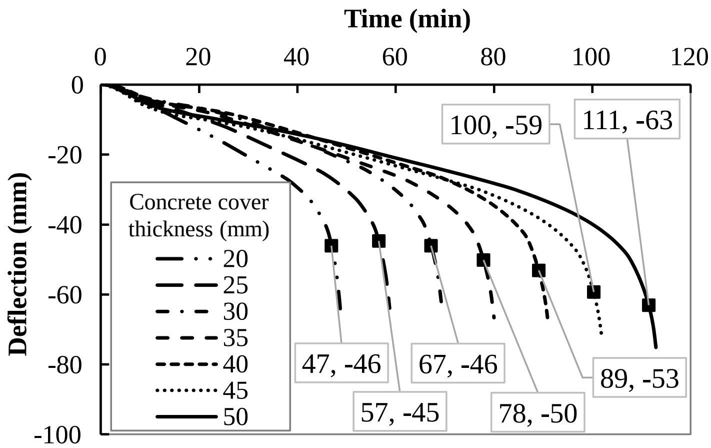

Figure 19. Deflection–time curves of beams with different concrete cover thicknesses

Figure 19 indicates that the increase in the thickness of concrete cover shifts the deflection–time curve rightward, increasing the fire resistance. Similar to the cases presented in the previous sections, the fire resistance of these beams was governed by the limit deflection rate, whereas the point corresponding to the deflection limit does not appear on the deflection–time curve. Figure 20 shows the variation in the fire resistance with respect to the thickness of concrete cover. The fire resistance of these beams increases linearly with the increase in the thickness of concrete cover. The beam with a concrete cover thickness of 20 mm had a fire resistance of 47 min. When the concrete cover thickness increased to 50 mm, the fire resistance was 111 min, which is approximately 1.5 times the fire resistance of a beam with a concrete cover thickness of 20 mm. On average, the fire resistance increases by ~2.15 min per 1 mm of the concrete cover thickness. This can be explained by the fact that the increases in the concrete cover thickness resulted in a slower increase in the temperature of GFRP/steel reinforcement, simply because of the larger distance to the concrete surfaces. Thus, it causes a slower degradation of strength, elastic modulus, and stiffness, contributing to increasing the longer fire resistance of the beams.

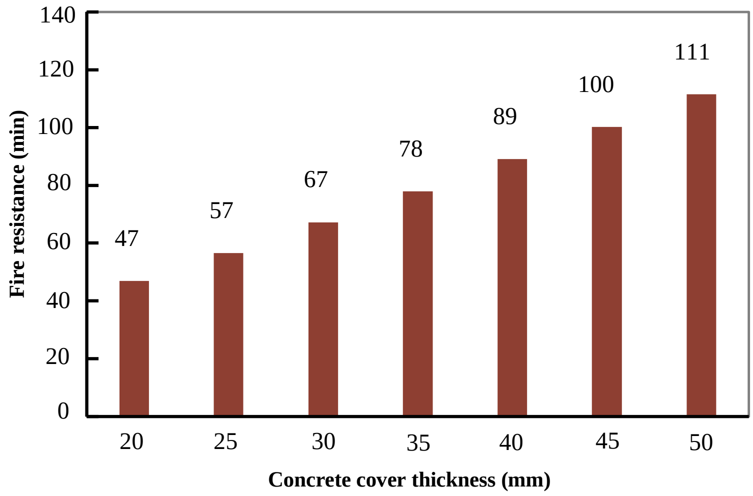

Figure 20. Variation in the fire resistance with respect to the concrete cover thickness

4.5. Effect of Yield Strength Steel on Deflection–Time Behavior

In this subsection, the effect of yield strength of steel on deflection–time behavior of RC beams was analyzed. These RC beams had the A_f/A ratio of 0.5, the total longitudinal reinforcement ratio ρ of 1.27, the concrete cover thickness of 20 mm, and the compressive strength of concrete of 30 MPa. The yield strengths of steel were 350, 450, 550, and 650 MPa. During the fire exposure, the beam was subjected to a constant concentrated load at the mid-span. The magnitude of the concentrated load was 40% of the ultimate load.

Figure 21 shows the variations in the deflection–time curves of the beams with different yield strengths of steel. Figure 21 indicates that the deflection–time curves are linear and almost identical during the first 30 min of fire. In this duration, the variation in yield strength of steel does not have any influence on the deflection–time behavior of the beams. The deflection–time curves start to deviate at 30 min. The increase in yield strength slightly shifts the curves rightward. Similar to the previous cases, the fire resistance was also governed by the deflection rate, while the deflection limit was not reach.

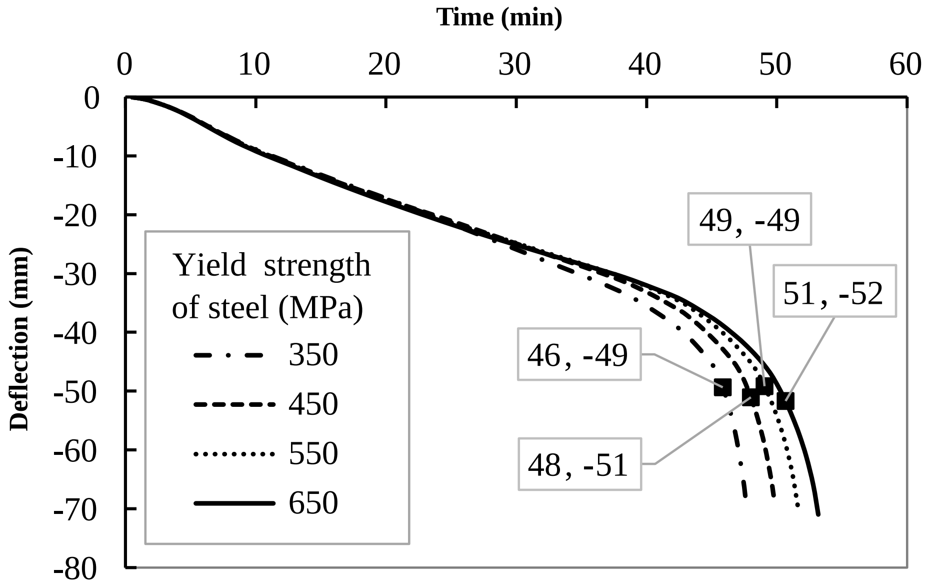

Figure 21. Deflection–time of beams with different yield strength of steel

Figure 22 shows the variation in the fire resistance with respect to the yield strength of steel. When increasing the yield strength from 350 MPa to 650 MPa, the fire resistance increased by only 5 min, corresponding to 10.9%. This negligible increase in the fire resistance can be explained by the fact that deflection depends on the elastic modulus, while the elastic modulus was 200 GPa, regardless of the yield strength of steel. Therefore, there would be a similar decrease in the elastic modulus during the fire exposure, resulting in no difference in deflection–time behavior, although the yield strength of steel was different.

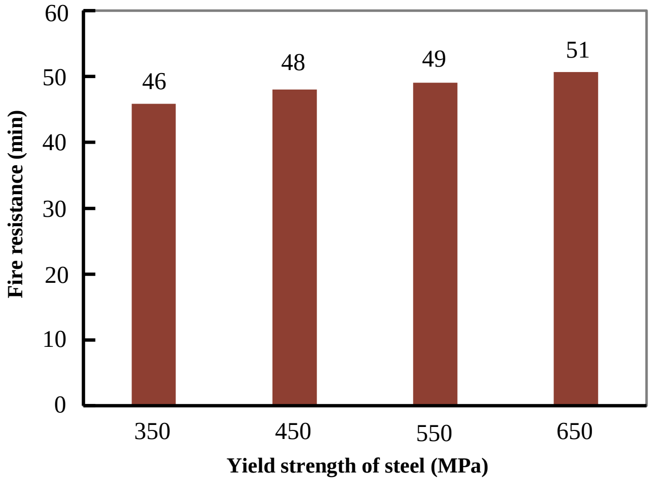

Figure 22. Variation in fire resistance with respect to the yield strength of steel

4.6. Effect of Concrete Strength

In this subsection, RC beams with different compressive strengths of concrete were analyzed. The reinforcement was 2ϕ18 steel bars and 2ϕ18 GFRP bars; the ratio A_f/A was 0.5; concrete cover thickness was 20 mm; and yield strength of steel was 350 MPa. The applied load was constant at 40% of the ultimate load during the fire exposure. These parameters were kept unchanged, while the compressive strengths of concrete were 20, 30, 40, and 50 MPa. The modulus of concrete was $E_c = 4730\sqrt{f_c'}$ [41]. Figure 23 shows the deflection–time curves of the beams with different compressive strengths of concrete. The curves are almost similar during the first 5 min of fire. After that, the increase in the concrete strength shifts the deflection–time curve downward and leftward. This resulted in a decrease in fire resistance when increasing the compressive strength of concrete. The linearity seems to be up to 40 min. After 40 min, the deflection–time curves deviated from their linearity and went to the nonlinear state and collapsed. Similar to the above cases, the limit deflection rate occurred prior to the limit deflection regardless of the compressive strength of concrete.

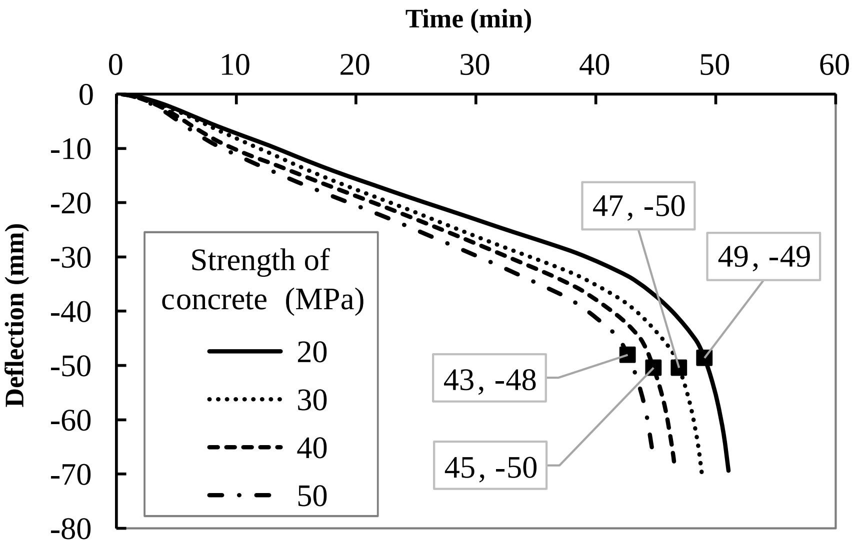

Figure 23. Deflection–time curves of beams with different compressive strengths of concrete

Figure 24 shows the variation in the fire resistance with respect to the compressive strength of concrete. The fire resistance of the beams exhibits an inverse correlation with the compressive strength of concrete. When the compressive strength increased from 20 MPa to 50 MPa, the fire resistance decreased from 49 min to 43 min, decreasing 12.2%. The decrease in the fire resistance with respect to the increase in the compressive strength of concrete can be explained as follows: Concrete with a higher compressive strength is more susceptible to high temperatures and has more cracks [42-44]. These cracks provide conditions for heat to transfer to the GFRP/steel bars faster, leading to a decrease in bond and stiffness. Thus, the hybrid GFRP-steel RC beams with a higher compressive strength of concrete failed earlier than those with a lower compressive strength of concrete.

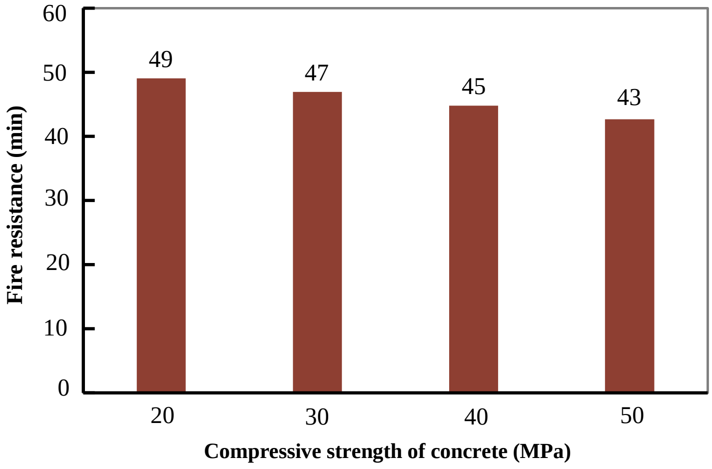

Figure 24. Variation in fire resistance versus the compressive strength of concrete

4.7. Effect of GFRP-Steel Arrangement on Deflection–Time Behavior

With a similar number of GFRP/steel bars, the arrangement of these bars on the beam cross sections can be different. Additionally, with a similar distance to the concrete surface, the temperature at corners is always higher than that at other positions because the corner positions are exposed to fire from two sides compared to one side at the other positions. Meanwhile, the loss of strength, elastic modulus, and the GFRP-concrete bond of GFRP bars are greater than those of steel bars when exposed to fire. Therefore, for hybrid GFRP-steel RC beams, positions of GFRP bars play an important role in the fire resistance of the hybrid beams. To consider the influence of the positions of GFRP bars on the fire resistance of beams, four arrangements of GFRP bars and steel bars on the beam cross section, as presented in Figure 25, are analyzed.

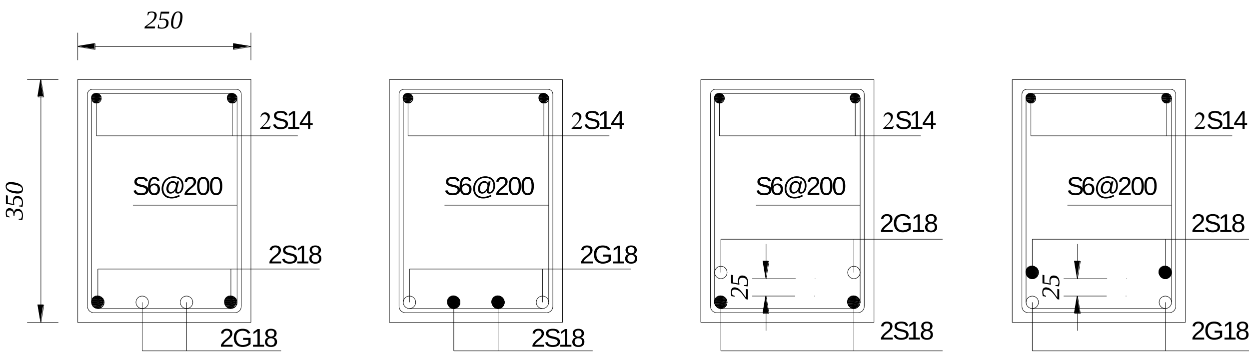

Figure 25. Locations of GFRP and steel bars

Figure 26 shows the deflection–time curves of the beams. Figure 26 indicates that the deflection rate limit always occurs prior to the deflection limit. In cases 1 and 3, the steel bars are arranged in a position with a higher temperature, while the GFRP bars are arranged inside locations with a lower temperature. The deflection–time curve of this beam goes through 3 stages: linear, nonlinear, and collapse. Meanwhile, in cases 2 and 4, the GFRP bars are arranged in a position with a higher temperature, then the deflection–time curve goes through 5 stages: linear, nonlinear, linear (repeated), nonlinear (repeated), and collapse. The first nonlinear stage is due to the deterioration of the strength and GFRP-concrete bond when the beam was exposed to fire, causing a slight-moderate increase in the deflection. This increase in the deflection is rather short, and it did not cause the beams to collapse. This is because the temperature of steel (located inside) is still lower, which helps the beams go to the third and the fourth phase — repeated linear and nonlinear phases. As the fire duration increases, the temperature in steel gradually increases, decreasing the mechanical properties and reinforcement-concrete bond. Consequently, the deflection gradually increases and then transitions to a nonlinear stage and collapses. The beam reinforced with GFRP bars arranged on the outer sides and steel arranged inside (case 4) has a deflection of 74 mm, which is the largest. Case 2 beam has the highest fire resistance of 65 min. Meanwhile, beams of cases 1 and 3 (steel bars arranged at the corners) have almost similar fire resistance and deflection. The fire resistance and deflection of beams in cases 1 and 3 are the lowest among the four cases.

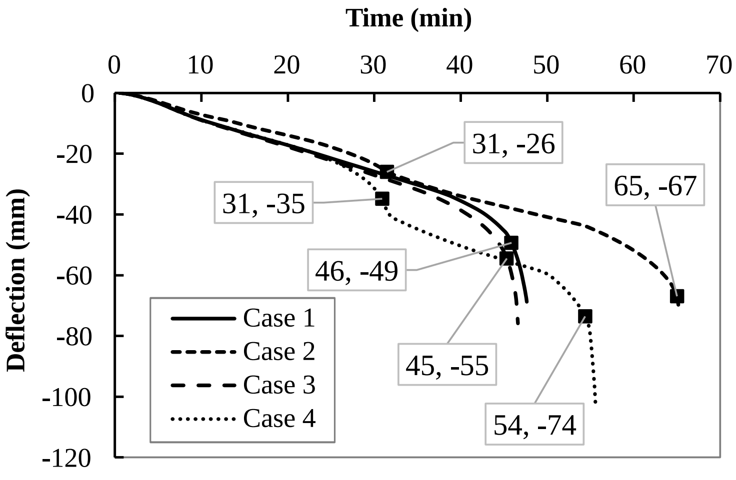

Figure 26. Deflection-time behavior of beams with different positions of GFRP bars on cross sections

Although the beams of cases 2 and 4 exhibited short nonlinear phases at the middle of the deflection–time curve, these beams still experienced the second linear phase. Therefore, the fire resistances of these beams were determined based on the deflection rate limit of the second nonlinear phase. Figure 27 presents the fire resistances for cases 1–4. The fire resistances of cases 1 and 3 are almost similar and are around 45 min. The fire resistance of the case 4 beam is 54 min. The highest fire resistance belongs to the case 2 beam, which is 65 min. These large variations in the fire resistance indicated that the locations of GFRP and steel bars play an important role in the fire resistance of hybrid GFRP-steel RC beams. This is attributed to the fact that, with a similar distance to the concrete surface, a point near corners has a higher temperature than any other points. Additionally, the reductions in the elastic modulus and strength of GFRP bars are higher than those of steel bars.

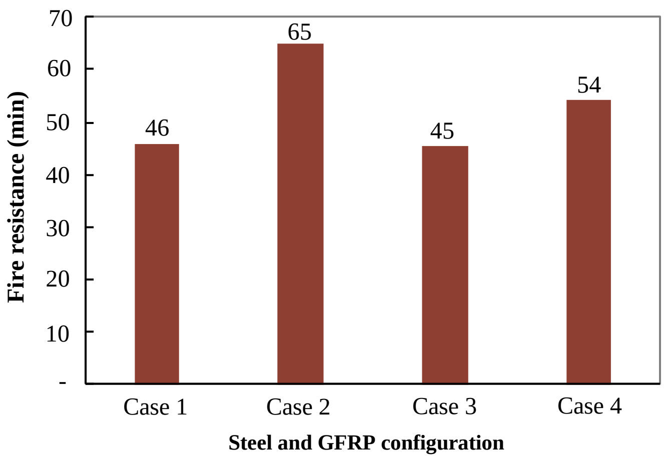

Figure 27. Fire resistance of beams with different locations of steel and GFRP bars

5. Multiple Linear Regression Analysis

Correlations between fire resistance and parameters of beams reinforced with various combinations of GFRP and steel were analyzed using R software. This software specializes in processing and analyzing statistical data with open-source code. In this software, the multivariate regression method results in models based on the Bayesian Model Average (BMA) method. The independent variables include $x_1 = A_f/A$, $x_2 = \rho$, $x_3 = P_a/P_u$, $x_4 = a_0$, $x_5 = f_y$, and $x_6 = f'_c$, while the dependent variable is fire resistance (F_R). The multivariate linear regression algorithm selected the four best models. These models are shown in Table 7, which is exported from R software. In Table 7, the first column shows the independent variables. Column 2 presents the probability of the regression coefficient of each variable. Only variables with a probability larger than zero are included in the model. If a variable has a regression coefficient of 0, that variable has no influence on the fire resistance. Column 3 presents the expected values, which are the average value of the regression coefficient for each variable. Column 4 shows the standard deviation of expected values. The next four columns show parameters of four models, namely models 1–4, which are expressed by Equations 9 to 12, respectively. The signs of the coefficients of the four models indicate that the A_f/A ratio, load ratio, and the compressive strength of concrete exhibited negative influence on the fire resistance. In contrast, the total reinforcement ratio, the concrete cover thickness, and yield strength of steel exhibited a positive influence on the fire resistance

Table 7. Results of multivariate regression analysis

	p!=0	Estimated Value	Standard deviation	Model 1	Model 2	Model 3	Model 4
Intercept	100.0	45.31	9.30	42.97	51.37	40.14	48.80
x_1	100.0	-60.29	5.68	-60.29	-60.29	-60.29	-60.29
x_2	100.0	14.81	3.03	14.86	14.61	15.05	14.78
x_3	100.0	-59.52	11.01	-59.60	-59.25	-59.86	-59.49
x_4	100.0	2.03	0.11	20.37	2.03	2.04	2.03
x_5	16.6	0.00	0.01	.	.	0.01	0.01
x_6	33.3	-0.09	0.17	.	-0.26	.	-0.26
Number of Variables				4	5	5	6
$\mathbf{R^2}$				0.945	0.948	0.946	0.949
Bayesian Information Criteria (BIC)				-81.76	-80.38	-78.56	-77.11
Posterior Probability				0.555	0.279	0.112	0.054

$$\text{Model 1: } F_R = -60.29(x_1) + 14.86(x_2) - 59.59(x_3) + 2.04(x_4) + 42.97 \tag{9}$$

$$\text{Model 2: } F_R = -60.29(x_1) + 14.61(x_2) - 59.25(x_3) + 2.03(x_4) - 0.26(x_6) + 51.37 \tag{10}$$

$$\text{Model 3: } F_R = -60.29(x_1) + 15.05(x_2) - 59.86(x_3) + 2.04(x_4) + 0.0068(x_5) + 40.14 \tag{11}$$

$$\text{Model 4: } F_R = -60.29(x_1) + 14.78(x_2) - 59.49(x_3) + 2.03(x_4) + 0.0058(x_5) - 0.26(x_6) + 48.8 \tag{12}$$

The last four rows of Table 7 present the number of variables, R^2, Bayesian Information Criteria (BIC), and posterior probability, respectively. Model 1 considered the first four variables x_1–x_4 while it excluded variables $x_5 = f_y$ (yield strength of steel) and $x_6 = f'_c$ (compressive strength of concrete). Models 2 and 3 additionally considered variables x_6 and x_5, respectively, while model 4 took into account all six parameters. The R^2 values of these four models are almost similar (~0.945). The BIC value of model 1 was the lowest (-81.76), followed by that of models 2 and 3, while that of model 4 is the highest (-77.11). The outstanding difference among the four models is the value of posterior probability. The posterior probability of model 1 is the highest (0.555), followed by that of models 2 and 3, while that of model 4 is the lowest (0.054).

The above results indicate that model 1 is the best model because it has the fewest variables while having the highest posterior probability. Four parameters of the A_f/A ratio, load ratio, total reinforcement ratio, and the concrete cover thickness have a significant influence on the fire resistance. In contrast, the yield strength of steel and the compressive strength of concrete negligibly affect the fire resistance. The above results also clearly confirmed the negligible influence of the yield strength of steel and the compressive strength of concrete.

6. Conclusions

The following conclusions are drawn:

- The deflection rate limit, instead of the deflection limit, decisively governed the fire resistance of concrete beams reinforced with various GFRP-steel combinations. This is attributed to the high reduction rates in the elastic modulus and strength of GFRP bars and steel bars.
- With a similar total reinforcement ratio, the increase in the ratio A_f/A reduces the fire resistance of hybrid GFRP-steel RC beams. When the A_f/A ratio is less than 0.5, the fire resistance decreases linearly with respect to the increase in the A_f/A ratio, and the decreasing rate in fire resistance is about 9 min per A_f/A ratio of 0.1 (on average). When this ratio is greater than 0.5, the decreasing rate in fire resistance decreases significantly up to 2.5 min per A_f/A ratio of 0.1.
- The load ratio and concrete cover thickness greatly increased the fire resistance of beams. When the load ratio increases from 0.1 to 0.6, the fire resistance decreases by about 45%. The fire resistance increased by 2.15 min per mm (on average) of the concrete cover thickness.
- The tensile strength of steel and the compressive strength of concrete had marginal effects on the fire resistance of beams reinforced with various combinations of GFRP and steel. When increasing the yield strength of steel from

350 MPa to 650 MPa, the fire resistance increases by only about 10.9%. When increasing the compressive strength of concrete from 20 MPa to 50 MPa, the fire resistance decreases by about 12.2%.

- When arranging GFRP at corners (where the temperature is higher), fire resistance is greater than in the case of arranging GFRP on the inside, although these beams experienced a short nonlinear stage at the middle of the curves. In contrast, when arranging GFRP bars on the inside (where the temperature is lower), beam deflection is smaller than when arranging GFRP bars on the outside. In this second arrangement, the deflection–time curve did not exhibit a short nonlinear stage at the middle of the curves.
- The results from the multivariate regression analyses proposed a model to predict the fire resistance of concrete beams reinforced with various combinations of GFRP and steel, including 4 parameters: A_f/A ratio, load ratio, total reinforcement ratio, and the concrete cover thickness. In this model, the first two parameters have a negative effect on the fire resistance of the beam; the remaining two parameters have a positive effect.

7. Declarations

7.1. Author Contributions

Conceptualization, V.V.C.; methodology, D.V.D.; software, D.V.D. and V.V.C.; validation, D.V.D. and V.V.C.; formal analysis, D.V.D.; investigation, D.V.D.; resources, D.V.D.; data curation, D.V.D.; writing—original draft preparation, D.V.D.; writing—review and editing, V.V.C.; visualization, V.V.C.; supervision, V.V.C.; project administration, V.V.C.; funding acquisition, V.V.C. All authors have read and agreed to the published version of the manuscript.

7.2. Data Availability Statement

The data presented in this study are available in the article.

7.3. Funding

This research is funded by Vietnam National University HoChiMinh City (VNU-HCM) under grant number: B2024-20-08.

7.4. Conflicts of Interest

The authors declare no conflict of interest.

8. References

[1] Zabihi-Samani, M., Shayanfar, M. A., Safiey, A., & Najari, A. (2018). Simulation of the Behavior of Corrosion Damaged Reinforced Concrete Beams with/without CFRP Retrofit. Civil Engineering Journal, 4(5), 958. doi:10.28991/cej-0309148.

[2] Djamaluddin, R., Irmawaty, R., Fakhruddin, & Yamaguchi, K. (2024). Flexural Behavior of Repaired Reinforced Concrete Beams Due to Corrosion of Steel Reinforcement Using Grouting and FRP Sheet Strengthening. Civil Engineering Journal (Iran), 10(1), 222–233. doi:10.28991/CEJ-2024-010-01-014.

[3] Ge, W., Zhang, J., Cao, D., & Tu, Y. (2015). Flexural behaviors of hybrid concrete beams reinforced with BFRP bars and steel bars. Construction and Building Materials, 87, 28–37. doi:10.1016/j.conbuildmat.2015.03.113.

[4] El Refai, A., Abed, F., & Al-Rahmani, A. (2015). Structural performance and serviceability of concrete beams reinforced with hybrid (GFRP and steel) bars. Construction and Building Materials, 96, 518–529. doi:10.1016/j.conbuildmat.2015.08.063.

[5] Pang, L., Qu, W., Zhu, P., & Xu, J. (2016). Design Propositions for Hybrid FRP-Steel Reinforced Concrete Beams. Journal of Composites for Construction, 20(4), 04015086. doi:10.1061/(asce)cc.1943-5614.0000654.

[6] Qin, R., Zhou, A., & Lau, D. (2017). Effect of reinforcement ratio on the flexural performance of hybrid FRP reinforced concrete beams. Composites Part B: Engineering, 108, 200–209. doi:10.1016/j.compositesb.2016.09.054.

[7] Barris, C., Torres, L., Turon, A., Baena, M., & Catalan, A. (2009). An experimental study of the flexural behaviour of GFRP RC beams and comparison with prediction models. Composite Structures, 91(3), 286–295. doi:10.1016/j.compstruct.2009.05.005.

[8] ACI 440.1R-06. (2005). Guide for the design and construction of concrete reinforced with FRP bars. American Concrete Institute (ACI), Michigan, United States.

[9] EN 1992-1-1. (2004). Eurocode 2: Design of concrete structures - Part 1-1 : General rules and rules for buildings European Committee for Standardization, Brussels, Belgium.

[10] Qu, W., Zhang, X., & Huang, H. (2009). Flexural Behavior of Concrete Beams Reinforced with Hybrid (GFRP and Steel) Bars. Journal of Composites for Construction, 13(5), 350–359. doi:10.1061/(asce)cc.1943-5614.0000035.

[11] Lau, D., & Pam, H. J. (2010). Experimental study of hybrid FRP reinforced concrete beams. Engineering Structures, 32(12), 3857–3865. doi:10.1016/j.engstruct.2010.08.028.

[12] Kara, I. F., Ashour, A. F., & Köroğlu, M. A. (2015). Flexural behavior of hybrid FRP/steel reinforced concrete beams. Composite Structures, 129, 111–121. doi:10.1016/j.compstruct.2015.03.073.

[13] Araba, A. M., & Ashour, A. F. (2018). Flexural performance of hybrid GFRP-Steel reinforced concrete continuous beams. Composites Part B: Engineering, 154, 321–336. doi:10.1016/j.compositesb.2018.08.077.

[14] Duic, J., Kenno, S., & Das, S. (2018). Performance of concrete beams reinforced with basalt fibre composite rebar. Construction and Building Materials, 176, 470–481. doi:10.1016/j.conbuildmat.2018.04.208.

[15] Abbas, H., Abadel, A., Almusallam, T., & Al-Salloum, Y. (2022). Experimental and analytical study of flexural performance of concrete beams reinforced with hybrid of GFRP and steel rebars. Engineering Failure Analysis, 138(106397). doi:10.1016/j.engfailanal.2022.106397.

[16] Yoo, D. Y., Banthia, N., & Yoon, Y. S. (2016). Flexural behavior of ultra-high-performance fiber-reinforced concrete beams reinforced with GFRP and steel rebars. Engineering Structures, 111, 246–262. doi:10.1016/j.engstruct.2015.12.003.

[17] Abdalla, H. A. (2002). Evaluation of deflection in concrete members reinforced with fibre reinforced polymer (FRP) bars. Composite Structures, 56(1), 63–71. doi:10.1016/S0263-8223(01)00188-X.

[18] Terzioglu, H., Eryilmaz Yildirim, M., Karagoz, O., Unluoglu, E., & Dogan, M. (2024). Flexural behavior of concrete beams hybrid-reinforced with glass fiber-reinforced polymer, carbon fiber-reinforced polymer, and steel rebars. Advances in Structural Engineering, 27(5), 775–795. doi:10.1177/13694332241232051.

[19] Dang Vu, H., Kawai, K., Dang, V. Q., & Nguyen Phan, D. (2025). The pre-cracked hybrid GFRP-steel RC beams strengthened with CFRP sheet: experiment and strength prediction. European Journal of Environmental and Civil Engineering, 2025, 1–24. doi:10.1080/19648189.2024.2448667.

[20] Adem Yimer, M., & Dey, T. (2024). Dynamic response of concrete beams reinforced with GFRP and steel bars under impact loading. Engineering Failure Analysis, 161(108329). doi:10.1016/j.engfailanal.2024.108329.

[21] Puzach, S., Liubov, L., Kamchatova, E., Nosova, L., Degtyareva, V., Tarasova, V., & Komarova, L. (2024). Development of a Method for Increasing the Fire Resistance of Cast-iron Structures of Cultural Heritage Sites under Reconstruction. Civil Engineering Journal (Iran), 10(2), 555–570. doi:10.28991/CEJ-2024-010-02-015.

[22] Shubbar, H. A., & Alwash, N. A. (2020). The fire exposure effect on hybrid reinforced reactive powder concrete columns. Civil Engineering Journal (Iran), 6(2), 363–374. doi:10.28991/cej-2020-03091476.

[23] Rafi, M. M., & Nadjai, A. (2011). Behavior of hybrid (steel-CFRP) and CFRP bar-reinforced concrete beams in fire. Journal of Composite Materials, 45(15), 1573–1584. doi:10.1177/0021998310385022.

[24] Rafi, M. M., & Nadjai, A. (2013). Numerical modelling of carbon fibre-reinforced polymer and hybrid reinforced concrete beams in fire. Fire and Materials, 37(5), 374–390. doi:10.1002/fam.2135.

[25] Tian, J., Zhu, P., & Qu, W. (2019). Study on fire resistance time of hybrid reinforced concrete beams. Structural Concrete, 20(6), 1941–1954. doi:10.1002/suco.201800320.

[26] Albu-Hassan, N. H., & Al-Thairy, H. (2020). Experimental and numerical investigation on the behavior of hybrid concrete beams reinforced with GFRP bars after exposure to elevated temperature. Structures, 28, 537–551. doi:10.1016/j.istruc.2020.08.079.

[27] Al-Thairy, H. (2020). A simplified method for steady state and transient state thermal analysis of hybrid steel and FRP RC beams at fire. Case Studies in Construction Materials, 13. doi:10.1016/j.cscm.2020.e00465.

[28] Hassan, A., Khairallah, F., Elsayed, H., Salman, A., & Mamdouh, H. (2021). Behaviour of concrete beams reinforced using basalt and steel bars under fire exposure. Engineering Structures, 238, 112251. doi:10.1016/j.engstruct.2021.112251.

[29] Saafi, M. (2002). Effect of fire on FRP reinforced concrete members. Composite Structures, 58(1), 11–20. doi:10.1016/S0263-8223(02)00045-4.

[30] Said, M., Hamdy, H., El-Sayed, A. A., & Khalil, M. M. (2024). Structural efficiency of concrete beams reinforced with hybrid reinforcement bars under thermal loads. Journal of Building Engineering, 92, 109678. doi:10.1016/j.jobe.2024.109678.

[31] Mamdouh, H., Mehany, M., Ibrahim, W. M., Mohamed, H. M., & Ali, A. H. (2024). Concrete contribution to shear resistance of GFRP-RC beams under fire exposure. Case Studies in Construction Materials, 21. doi:10.1016/j.cscm.2024.e04109.

[32] Cao, V. Van, & Nguyen, V. N. (2022). Flexural Performance of Postfire Reinforced Concrete Beams: Experiments and Theoretical Analysis. Journal of Performance of Constructed Facilities, 36(3), 04022029. doi:10.1061/(asce)cf.1943-5509.0001739.

[33] Nigro, E., Bilotta, A., Cefarelli, G., Manfredi, G., & Cosenza, E. (2012). Performance under Fire Situations of Concrete Members Reinforced with FRP Rods: Bond Models and Design Nomograms. Journal of Composites for Construction, 16(4), 395–406. doi:10.1061/(asce)cc.1943-5614.0000279.

[34] Rosa, I. C., Firmo, J. P., Correia, J. R., & Bisby, L. A. (2023). Fire Behavior of GFRP-Reinforced Concrete Structural Members: A State-of-the-Art Review. Journal of Composites for Construction, 27(5), 03123002. doi:10.1061/jccof2.cceng-4268.

[35] Gernay, T., & Franssen, J. M. (2012). A formulation of the Eurocode 2 concrete model at elevated temperature that includes an explicit term for transient creep. Fire Safety Journal, 51, 1–9. doi:10.1016/j.firesaf.2012.02.001.

[36] Song, Y., Fu, C., Liang, S., Yin, A., & Dang, L. (2019). Fire Resistance Investigation of Simple Supported RC Beams with Varying Reinforcement Configurations. Advances in Civil Engineering, 8625360. doi:10.1155/2019/8625360.

[37] Song, Y., Fu, C., Liang, S., Li, D., Dang, L., Sun, C., & Kong, W. (2020). Residual Shear Capacity of Reinforced Concrete Beams after Fire Exposure. KSCE Journal of Civil Engineering, 24(11), 3330–3341. doi:10.1007/s12205-020-1758-7.

[38] GangaRao, H. V. S., Taly, N., & Vijay, P. V. (2006). Reinforced Concrete Design with FRP Composites. CRC Press, Boca Raton, United States. doi:10.1201/9781420020199.

[39] Yu, B., & Kodur, V. K. R. (2013). Factors governing the fire response of concrete beams reinforced with FRP rebars. Composite Structures, 100, 257–269. doi:10.1016/j.compstruct.2012.12.028.

[40] BS EN 1363-1:2020. (2020). TC Fire resistance tests - General requirements. British Standard (BSI), London, United Kingdom.

[41] Park, R., & Paulay, T. (1991). Reinforced concrete structures. John Wiley & Sons, Hoboken, United States.

[42] Kodur, V. K. R. (2004). Spalling in high strength concrete exposed to fire - Concerns, causes, critical parameters and cures. Structures Congress 2000: Advanced Technology in Structural Engineering, 103, 1–9. doi:10.1061/40492(2000)180.

[43] Kodur, V. K. R., & Dwaikat, M. (2007). Performance-based fire safety design of reinforced concrete beams. Journal of Fire Protection Engineering, 17(4), 293–320. doi:10.1177/1042391507077198.

[44] Dwaikat, M. B., & Kodur, V. K. R. (2009). Response of Restrained Concrete Beams under Design Fire Exposure. Journal of Structural Engineering, 135(11), 1408–1417. doi:10.1061/(asce)st.1943-541x.0000058.